Antibacterial surfaces prepared by electrospray coating of photocatalytic nanoparticles

Please, cite as follows:

Blanca Jalvo, Marisol Faraldos, Ana Bahamonde, Roberto Rosal, Antibacterial surfaces prepared by electrospray coating of photocatalytic nanoparticles, In Chemical Engineering Journal, 334, 1108–1118, 2018, ISSN 1385-8947, https://doi.org/10.1016/j.cej.2017.11.057.

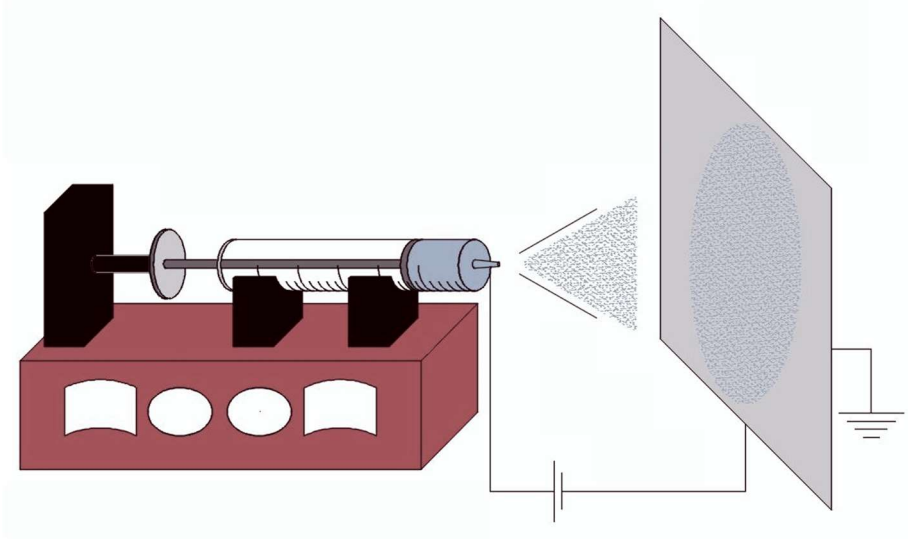

http://www.sciencedirect.com/science/article/pii/S1385894717319708

Antibacterial surfaces prepared by electrospray coating of photocatalytic nanoparticles

Blanca Jalvo[1], Marisol Faraldos[2,*], Ana Bahamonde[2], RobertoRosal[1,*]

[1] Department of Chemical Engineering, University of Alcalá, E-28871 Alcalá de Henares, Madrid, Spain
[2] Instituto de Catálisis y Petroleoquímica, ICP-CSIC, Marie Curie 2, E-28049 Madrid, Spain

* Corresponding authors: mfaraldos@icp.csic.es, roberto.rosal@uah.es

Abstract

The aim of this work was to use electrospray to create photocatalytic TiO_2 coatings and to study their antibacterial and antibiofilm capacity. The electrospray used a sol of TiO_2 anatase nanoparticles prepared by a sol-gel method, which formed stable suspensions of positively charged particles (ζ-potential +22.3 ± 3.7 mV). The electrospray deposited TiO_2 on non-porous glass surfaces at two loading densities originating homogeneous coatings (3.2-4.3 μm) of particles the top layer of which displayed aggregates ranging from the micron scale to a few hundreds of nanometers, with lower size as TiO_2 loading increased. TiO_2-functionalized surfaces were tested for the inactivation of the Gram-positive bacterium *Staphylococcus aureus*. The electrosprayed surface was moderately hydrophilic turning highly hydrophilic upon irradiation (water contact angle 9.6° after 15 h under Xe-arc lamp). photocatalytic surfaces were put in contact with exponentially growing bacterial cultures in a flow system in which solar simulated irradiation followed two different 24 h dark-light arrangements with 9 or 18 h dark exposure followed by 15 or 6 h irradiation. The electrosprayed surfaces experienced extensive colonization by viable bacteria and clear biofilm formation revealed by exopolysaccharide matrix visualization. Using both dark-light cycles all cells became non-viable with extensive membrane damage. Biofilm matrix measurements showed that the irradiated surfaces were essentially free of bacterial exopolysaccharide matrix for specimens with the higher TiO_2 loading density. The biofilm removal reached 99% and no regrowth of viable cells was observed in any case. The results showed that TiO_2-electrospray can avoid biofilm accumulation under stringent environmental conditions.

Keywords: Electrospray; Solar Photocatalysis; Titanium dioxide; Antibacterial Surface; Self-Cleaning Materials; Bacterial Biofilms

1. Introduction

In the last 25 years, photocatalytic titanium dioxide (TiO_2) has been extensively studied for the removal of pollutants from water and air among other environmental applications [1,2]. When TiO_2 surfaces are photoexcited by near-ultraviolet light (UV-A, wavelengths 320–400 nm) electrons from the valence band migrate to the conduction band, forming e^-/h^+ pairs that generate, in the presence of water and oxygen, oxidants species like hydroxyl radical, hydrogen peroxide and superoxide anion, which apart from removing pollutants convey biocidal activity [3,4]. TiO_2 itself is non-toxic for human beings, relatively inexpensive, environmentally friendly, chemically stable and effective under weak solar irradiation in atmospheric environments [5-7]. The antimicrobial properties of photoactivated TiO_2 have been explored for a number of cell types, either in suspended form or supported on different substrates [8-11]. The biocidal activity of TiO_2 is triggered by the well-known oxidative damage of cell membranes [12]. The photocatalytic oxidative activity induces rapid cell inactivation at the regulatory and signaling levels, impairs coenzyme dependent and independent enzyme activities, and alters the metabolisms of micronutrients [13]. Yoon et al. [14] prepared titanium dioxide films by electrostatic spray, which showed photocatalytic activity through the degradation of methylene blue and against the bacterium *Escherichia coli* under UV light. The effect was attributed to the formation of anatase polycrystalline phase upon annealing at 500 °C. However, only a few publications addressed the specific subject of biofilm formation on photocatalytic TiO_2. Clearly an increase in the intensity of the photocatalytic processes leads to a decrease in bacterial adhesion to TiO_2 functionalized surfaces [15]. Gage et al. [16] found that bacteria in biofilms were not significantly impaired by the photocatalytic activity of UV irradiated TiO_2, the effect being similar to that of UV alone. The reasons for the lack of photocatalytic effect on attached cells is the protection offered by extracellular substances that avoid the direct contact between cells and the photocatalytic surface, the specific responses from attached cells that impart resistance to the reactive oxygen species generated through photocatalytic oxidation or the scavenging of reactive radicals. However, Ciston et al. [17] proved that photocatalytic TiO_2 coatings reduced bacterial cell

attachment and allowed long-term control of biofilm formation in water filtration ceramic membranes.

Electrospray is a method that produces micron sized droplets from a nozzle tip by applying an electric field [18]. Together with electrospinning constitutes a field known as electrohydrodynamic techniques, which transform liquid droplets into nanomaterials using strong electric fields. While electrospraying refers to the formation of nanoparticles, electrospinning describes the fabrication of fibrous structures [19]. In electrospray, the suspension flowing out from a nozzle is forced to disperse into fine droplets by the electric field created by a high voltage source. The size of electrosprayed droplets ranges from hundreds of micrometers down to several tens of nanometers depending on the physical properties of the suspension, the liquid flow rate and the voltage applied between nozzle and collector [18,20,21]. Electrospray has been studied as a novel powder-processing method that, combined not with pyrolysis, attracted considerable attention as a method of preparation of functional submicrometer particles [22,23]. Electrospray is also a technique for thin film deposition suitable to prepare solid coatings of nanodispersed particles from the aerosol phase on a wide variety of surfaces, with the advantage of being easily scaled-up to industrial processes from laboratory data [24]. Surfaces functionalized with electrosprayed TiO_2 find application, among other uses, as photoelectrodes in dye-sensitized solar cells [25,26], the removal or organic pollutants by exploiting the possibility of creating highly dispersed hierarchical structures with photocatalytic activity [27] and the creation of ceramic films to protect metallic surfaces against high temperature and erosion stresses [28]. The films formed by electrospray have the advantage of displaying a high degree of uniformity that, dependent of the parameters governing the droplet evaporation rate, can produce films with high degree of interconnectivity and good mechanical properties [29].

Staphylococcus aureus is a prominent nosocomial pathogen and a major cause of infections associated to bacterial colonization and biofilm formation on different kinds of surfaces including those related to healthcare-associated infections. The success of *S. aureus* as a pathogen is due in part to its ability to adapt to stressful environments [30]. One adaptation strategy is biofilm formation. Biofilms are communities of cells embedded in an extracellular polymeric matrix formed by polysaccharides, proteins, and nucleic acids, which protect cells from adverse conditions [31]. Biofilms are highly structured multispecies communities with integrated metabolic activities and structural adaptations that include altered phenotypes, which evolved to create their own environment. Biofilms are of particular concern due to their resistance to conventional disinfecting agents and because they are very difficult to remove once initial adhesion occurs [32]. It has been shown that the control of biofouling requires the prevention of initial bacterial attachment. Once formed, the polymeric extracellular matrix of biofilms acts as protective barrier against oxidative radicals and cannot be removed even under conditions that lead to extensive cell damage. This highlights the importance of avoiding bacterial colonization during dark periods or non-irradiated areas in view of the difficulty of removing the structure of mature biofilms. [33].

In this work the electrospray technique has been used to produce TiO_2-coated surfaces from suspensions of nanoparticles prepared by means of a non-thermal sol-gel process. The use of electrospray to create antimicrobial TiO_2-functionalized surfaces has been seldom reported in the literature, with some references exploring the combination of electrospray and electrospinning to create hierarchically structured functional nanofibers [34]. The main goal was to investigate its photocatalytic antimicrobial and antibiofilm activity against *S. aureus*. The photocatalytic materials were allowed to develop biofilms in the dark prior to irradiation with a visible light source. TiO_2-functionalized surfaces with different surface densities were used, which were irradiated for two different light-dark cycles to emulate different solar irradiation conditions. Contrary to the usual testing of antimicrobial surfaces, the assays were carried out under continuous flow and the attention was focused on the removal of biofilm polymeric matrices grown during the dark part of the cycle.

2. Materials and methods

2.1. Photocatalytic materials

Crystalline anatase nanoparticles were prepared by a sol-gel synthesis. The procedure used to prepare both TiO_2 suspensions was described in detail previously [35]. Briefly, 1.43 mL of concentrated nitric acid (Panreac 65%) were mixed with 100 mL of deionized water by vigorous stirring. Then, 16.5 mL of titanium isopropoxide (Sigma-Aldrich 97%) were added dropwise. The proportion of nitric acid and titanium isopropoxide was increased to 2.86 mL and 32 mL, respectively, in the case of the TiO_2 suspension with higher anatase content. The mixture was kept closed and moderately stirred for at least three days or until complete peptization, which was assessed by the change in the initially white precipitate into a translucent suspension. The translucent sol was transferred to a glass bottle and stored in the dark before electrospray. No other conditioning was performed as the presence of organic volatile solvents do not interfere with electrospray and high conductivity is an advantage for the electrohydrodynamic process.

For other applications a dialysis (3500 MWCO) cleaning procedure is commonly carried out using deionized water until TOC < 1 mg L^{-1}. The fact that this post-conditioning step is not required is an important advantage for electrospray.

2.2. Characterization of nanoparticle suspensions

Two different TiO_2 nanoparticle suspensions (TiO_2 A and TiO_2 B) were prepared and characterized using Dynamic Light Scattering (DLS) for particle size analysis and zeta potential (ζ-potential) measured via electrophoretic light scattering in a Zetasizer Nano ZS (Malvern Instruments, Malvern, UK) equipment. Surface ζ-potential was measured using the Capillary Zeta Cell DTS 1070 from Malvern. The pH and electrical conductivity of the suspensions were measured using a multimeter (Crison MM 40+). Surface tension was determined using the pendant drop method by means of an optical contact angle meter (Krüss DSA25 Drop Shape Analysis System) and the Java open source ImageJ software [36]. Band-gap was calculated from Tauc plots by means of UV–vis Diffuse Reflectance Spectroscopy using an Agilent Cary 5000 apparatus. Powder X-ray Diffraction was carried out in an PANalytical X'Pert Pro equipment, which allowed the characterization of crystalline phases and the estimation of crystallite size.

2.3. Electrospray of TiO_2 nanoparticles

Fig. 1 presents a schematic illustration of the experimental setup used for the electrospray (ES) TiO_2 coating. Before the ES process, the TiO_2 nanoparticle suspensions were sonicated using an ultrasonic probe VC505 (500W, Sonics and Materials Inc.) for 10 min in 30 s intervals at 20% amplitude followed by 10 min of magnetic stirring. The ES equipment consisted of a Heinzinger LNC 30000 high voltage power supply and a Harvard PHD PHD22/2000 syringe pump. The suspensions were deposited into a 5 mL syringe with a 23-gauge (nominal inner and outer diameters 0.337 and 0.641 mm) stainless steel blunt-tip needle at its end, which was connected to the high voltage power supply to create the required electric field. The voltage used was 19 kV and the flow rate was 0.1 mL h^{-1}. Electrosprayed drops were deposited on 13 mm diameter round glass coverslips (VWR, Germany), attached to a flat collector (16 cm x 16 cm aluminum grid) separated 10 cm from the needle tip. The flat collector and the needle were horizontally arranged to avoid gravity deposition. The parameters, voltage, flow rate and distance from needle tip to collector were determined based on the physicochemical characterization of the TiO_2 suspensions as described in the literature and by considering the scaling laws [37-40]. In particular, a low flow rate was used to avoid the corona effect, which would difficult Taylor cone formation and voltage and the distance to the collector plate were determined based on the previously mentioned parameters. TiO_2 nanoparticle suspensions were sprayed for 2 and 4 h in order to obtain two different surface coating densities. No polymer or other additives were added to the ES solution. Before and after ES coating, the cover supports were dried at 50° C for 1 h and accurately weighted to assess the amount of deposited photocatalytic material.

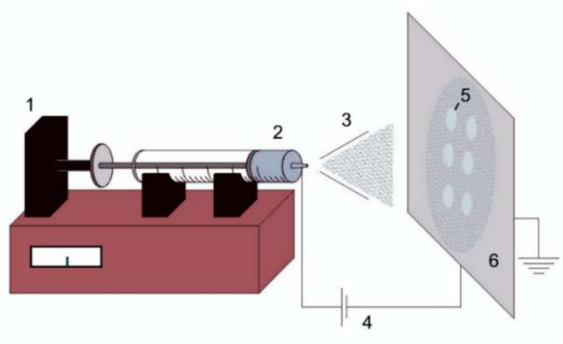

Figure 1. Schematic illustration of the electrospray setup for TiO_2 coating. (1) Syringe pump, (2) TiO_2 nanoparticle suspensions in a 5 mL syringe, (3) TiO_2 electrospray, (4) High voltage power supply, (5) Glass coverslips coated with electrosprayed TiO_2 electrospray, (6) Grounded collector.

2.4. Characterization of electrosprayed surfaces

Uncoated and electrosprayed TiO_2 coated surfaces were observed with scanning electron microscopy (SEM, Philips XL 30 S-FEG). Each sample was sputter-coated with gold prior to analysis. Cross-sectional micrographs were taken on specimens carefully cut using a diamond knife. The wettability of the surfaces was characterized using the optical contact angle meter Krüss DSA25 Drop Shape Analysis System described in a previous section by means of the sessile drop technique. Samples of functionalized and non-functionalized glass coverslips were placed on the test cell and Mili-Q water drops were deposited on them by the delivering syringe. Water contact angle (WCA) values were an average of at least three measurements on different positions of each surface. WCA measurements were taken at room temperature.

2.5. Photocatalytic bioassays

The bacterial strain used in this study to test the antibacterial activity of TiO_2 photoactivated materials was *Staphylococcus aureus* (CECT 240, strain designation ATCC 6538P). *S. aureus* was grown overnight in Nutrient Bacterial medium (NB, for 1 L solution in distilled water, beef extract 5 g, peptone 10 g, NaCl 5 g, pH adjusted to 7.2) while shaking at 37 °C. The temperature for bacterial pre-incubation was set following the usual microbiological procedures considering the well-known fact that *S. aureus* grows rapidly in aerated broth culture at 37° C [41]. The bioassays were performed using a flow-cell system as described elsewhere with some modifications [42,43].

Briefly, biofilm growth was allowed for 9 h or 18 h in darkness on the surface of coated and uncoated coverslips kept in flow chambers 5 mm depth, 25 mm width and 50 mm length provided by Sigma-Aldrich. Three coated or uncoated circular coverslips were placed in each flow-cell and a total amount of six flow-cells were used at the same time (Fig. 2). The entire flow system was connected by standard PVC tubing (1/16“ ID x 1/8” OD, Sigma-Aldrich), except for the tubing going through the peristaltic pump, which was silicone 1/8“ ID x 1/4” OD from Cole-Parmer. The circulating liquid was inoculated with exponentially growing cultures of *S. aureus* diluted in NB medium to an OD_{600} of 0.0138 (10^8 cells mL^{-1}). The feed bottle was maintained in a water bath incubator at 30 °C and the liquid culture was pumped using a peristaltic pump (Watson-Marlow, 101 U/R) at a constant rate. The incubation temperature was chosen to avoid nutrient depletion during the assay because *S. aureus* is a fast-growing microorganism. The temperature (30 °C) was set to allow performing antimicrobial tests under flow conditions without nutrient depletion inside for the 24 h periods indicated below at the same time keeping a high microbial growth rate. The linear velocity of the liquid through the flow-cells was 0.5 mm s^{-1}kept constant along the experiments. Immediately after the dark period of biofilm formation, the samples were continuously irradiated for 15 h or 6 h (to complete 24 h in all cases) using a simulated solar irradiation provided by a Heraeus TQ Xe 150 Xe-arc lamp at a distance of 15 cm from the flow-cells. This lamp has a light spectral distribution comprising wavelengths shorter than 300 nm (UV-C range) and between 300 and 400 nm (UV-B/-A range). The 290-400 nm range was 5.8% of the total output, while the visible part of the spectrum (400-700 nm) supposed 94.2% > 400 nm of the total radiant power emitted by the lamp. Fluence rate, measured in the 290-400 range, was 11.2 W m^{-2} as determined using 2-nitrobenzaldehyde as chemical actinometer [44].

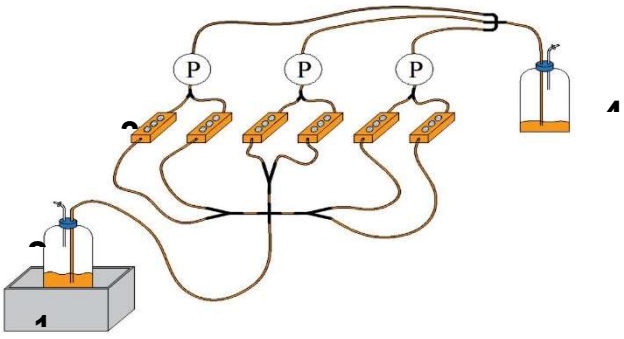

Figure 2. Schematic illustration of the flow-cell systems for photocatalytic bioassays. (1) Thermostatic water bath. (2) Feed tank with *S. aureus* culture. (3) TiO_2 coated/uncoated coverslips inside of the flow-cell chambers. (4) Effluent culture. P: Peristaltic pump. (Xe-Arc irradiation lamp not shown for clarity.)

2.6. Bioanalytical procedures

After completing the photocatalytic assays consisting of biofilm formation and irradiation treatment as described before, the coverslips were transferred to 24-well polystyrene plates. The biofilm was quantified based on optical density measurements following a modification of the method of Fletcher as described elsewhere [45,46]. For it, approximately 200 µL of a crystal violet 0.1% solution were extended over the washed surface of each coverslip and incubated for 15 min in order to allow the staining of adhered cells. Excess stain was eliminated by rinsing with distilled water. Plates were air dried and 1 mL of 95% ethanol was added to each well in order to extract crystal violet from cells. Distaining was performed overnight while gently shaking. Finally, the dye was measured at OD_{590}. Every measurement was performed at least three times for each experimental condition.

Bacterial viability assays were performed using Live/Dead BacLight Bacterial Viability Kit (ThermoFisher, Waltham, MA, USA). Under Live/Dead staining, all cells exhibit green fluorescence (SYTO 9), whereas nonviable bacterial cells display red fluorescence (Propidium iodide, PI) with dye uptake depending upon cell membrane integrity. For the staining of films 10µL of BacLight stain (a mixture of SYTO 9 and PI in DMSO, according to the manufacturer’s recommendations) were used. The incubation was performed in the dark for 15-30 min at room temperature. For green fluorescence (SYTO 9) excitation was performed at 488 nm and emission at 500-575 nm. For red fluorescence (PI, dead cells), the excitation/emission wavelengths were 561 nm and 570-620 nm respectively.

In order to visualize the extracellular polymeric matrix, the biofilms were stained with 200 µL FilmTracer SYPRO Ruby (Molecular Probes, Invitrogen) per sample, incubated in the dark for 30 min at room temperature, and rinsed with distilled water. Then, the coverslips were observed using confocal microscopy (Confocal SP5, Leica Microsystems, Germany) with excitation/emission wavelengths of 450 nm and 610 nm respectively. For all bioassays, independent runs were performed together with their respective controls.

3. Results and Discussion

3.1. Electrospray parameters

During electrospray, a conductive liquid is pumped at certain flow rate through a tube, forming a meniscus at its end. Due to the electrical field, the free charge in the conductive liquid meniscus generates an electric stress that opposes surface tension and forces the meniscus to a conical shape [37]. The liquid jet eventually breaks into drops due to capillary instabilities, giving rise to an aerosol of charged droplets [38]. The droplet diameter

is mainly depending on liquid conductivity and range from hundreds of micrometers to a few nanometers, with lower sizes for the more conducting liquids and a minor influence of the injected flow rate or voltage [39,40]. Surface tension is the other important parameter as electrospray takes place only when the coulomb repulsion is strong enough to overcome the liquid surface tension [21]. Table 1 shows the properties of the electrospray suspensions used in this work including electrical conductivity, surface tension. surface charge at the pH of bioassays, particle ζ-potential at the electrospray conditions and XRD parameters. XRD results (Fig. 3) demonstrated the only presence of anatase phase in both suspensions, even when the sol was not heat-treated. The formation of crystalline nanoparticles of anatase in acidic media has been previously described, the continuous and prolonged moderate stirring during several days allowing the initial precipitate to peptize and crystalize [35]. The crystallite size was calculated by Scherrer equation, and a comparable size was obtained: 4.3 nm for TiO_2 A (20 wt%) and 4.4 nm for TiO_2 (B) 40 wt%, clearly unaffected by the different loading of titanium dioxide. UV-Vis-NIR spectra (Fig. S1, Supplementary Material) showed similar shape with different intensities. Higher TiO_2 loading in the original suspension led to lower reflectivity along the observed region. The UV-Vis Diffuse Reflectance spectrum of photocatalyst xerogel (Fig. S2, Supplementary Material) showed that the photocatalyst absorption was mostly in the UV region of the spectrum.

Table 1. Properties of TiO_2 suspensions

TiO_2 A	
TiO_2 content	20 ± 4 wt%
Electrical conductivity	$2.39 \cdot 10^4$ ± 0.03 μS cm^{-1}
Surface tension	45.0 ± 0.7 mN m^{-1}
Surface ζ-potential (pH 7.0, mV)	+1.2 ± 0.7 mV
ζ-potential electrospray (pH 1.0, mV)	+26.2 ± 4.2 mV
Particle diameter (DLS, pH 1.0)	13.5 ± 0.9 and 88.7 ± 1.6 nm
Crystallite diameter (XRD, Scherrer)	4.3 ± 0.5 nm
TiO_2 B	
TiO_2 content	40 ± 7
Electrical conductivity	$3.47 \cdot 10^4$ ± 0.03 μS cm^{-1}
Surface tension	37.7 ± 0.4 mN m^{-1}
Surface ζ-potential (pH 7.0, mV)	+0.7 ± 0.8 mV
ζ-potential (electrospray, pH 1.0, mV)	+22.3 ± 3.7 mV
Particle diameter (DLS, pH 1.0)	15.8 ± 1.4 and 842 ± 85 nm
Crystallite diameter (XRD, Scherrer)	4.4 ± 0.5 nm

The pH of the electrosprayed suspension was 1.0 ± 0.2 at which, the ζ-potential of TiO_2particles was positive, +26.2 ± 4.2 and +22.3 ± 3.7 mV for 20 and 40 wt% suspensions respectively (TiO_2 A and B in Table 1). The stability of the colloidal system was assessed by measuring particle size (DLS) during a 4 h period that corresponded to the maximum electrospray time. Specifically, DLS results displayed peaks at 13.5 ± 0.9 (TiO_2 A) and d 15.8 ± 1.4 (TiO_2 B) that could be attributed to the primary particles of the TiO_2 suspension. Both TiO_2 suspensions revealed the formation of agglomerates, larger for the more concentrated one, which are probably in in dynamic equilibrium with the more numerous primary particles, which largely dominated the particle number distributions. Fig. S3 (Supplementary Material) shows detailed DLS measurements of TiO_2 A and TiO_2 B suspensions performed 10 min after the initial stirring and then every hour during a 4 h period. The deviation between XRD and DLS sizes is inside the usual discrepancies found in non-strictly unimodal samples. The reason is that the diameter obtained by DLS represents that of the hydration sphere, which is larger than that of naked particles, particularly in cases of high charge density.

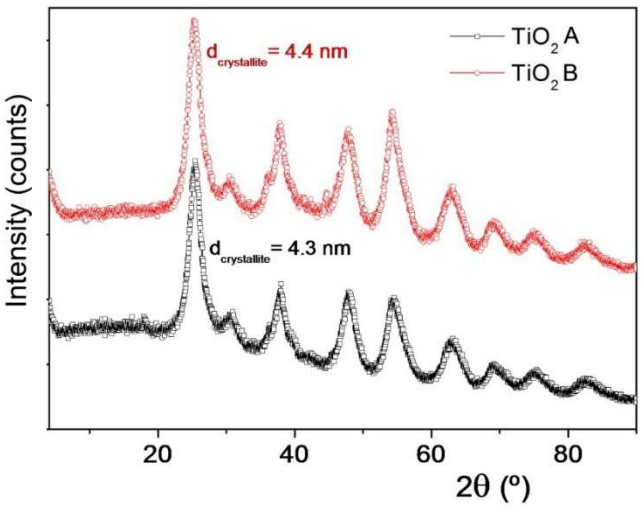

Figure 3. X-ray diffractograms of TiO_2 A and B xerogels.

The increase in TiO_2 concentration from 20 to 40 wt% (A to B) in the electrospray suspension decreased surface tension (-16%) and increased electrical conductivity (+60%) that can be explained by the presence of 2-propanol from the alkoxide precursor hydrolysis and nitrate ions from the reaction media. The simultaneous increase of ionic strength, which tends to compress the double layer of charged particles and reduces its mobility also explain the slightly lower values of ζ-potential of the TiO_2 B suspension. It is a well-known fact that water solutions are not directly suitable for electrospraying due to their high surface tension [18,37,47]. In the case of the TiO_2 A (20 wt%)

suspension the surface tension was 45.0 mN m^{-1}, which decreased to 37.7 mN m^{-1} for the TiO_2 B (40 wt%), which was enough to allow electrospraying without the use of surfactants. The TiO_2 B suspension was the material of choice in this work and all results explained below were obtained with it.

3.2. TiO_2 nanoparticle electrospray coatings

The ES process was performed using two different spray times (of TiO_2 B) that led to two different TiO_2 loadings on the surface of glass coverslips. The nomenclature used for the electrosprayed samples and the values obtained for the surface density of TiO_2 and water contact angle (WCA) on the surface of bare and coated coverslips are shown in Table 2. The mean loading density of samples with higher electrospray time, denoted as C(++), was 1/3 over those with lower TiO_2 amount, C(+). The WCA on the surface of neat glass coverslips, without TiO_2 coating, C(-), was 75.2°± 2.8°, less hydrophilic that that of TiO_2 coated surfaces, for which WCA measured on non-irradiated samples decreased to values in the 55-60° range. The wettability increased considerably and led to clearly hydrophilic surfaces upon irradiation. WCA dropped to values around 20-30°, after 6 h of irradiation treatment, and less than 10° after 15 h under Xe-arc lamp. The WCA were lower for C(++) samples, but the difference was not significant.

Table 2. Loading density of TiO_2 on electrosprayed samples and WCA measurements.

	Bare coverslips	Low loading	High loading
Identifier	C(-)	C(+)	C(++)
TiO_2 surface density (mg cm^{-2})	-	2.09 ± 0.12	2.78 ± 0.23
WCA (°), non-irradiated	75.2 ± 2.8	59.3 ± 2.7	56.4 ± 2.1
WCA (°), irradiated 6 h	73.7 ± 2.1	28.5 ± 1.5	21.2 ± 3.3
WCA (°), irradiated 15 h	75.4 ± 2.6	11.6 ± 2.2	9.6 ± 1.3

The decrease in WCA of TiO_2 exposed to UV light has been extensively documented from the early discovery of Wang et al. [48] who found that polycrystalline anatase decreased WCA from to zero after exposure to ultraviolet irradiation, particularly in the presence of water vapor. From then, the hydrophilic-hydrophobic transition induced by light of different wavelengths has been documented for many titanium dioxide surfaces [49,50]. The contact angle of water on a clean TiO_2 surface can be repeatedly cycled between practically zero, after UV irradiation or 50-60° after exposure to visible light to their initial values, which recovered after dark storage [51]. This photo-induced wettability transition has been attributed to the breaking of Ti─O lattice bonds by photogenerated holes. Water molecules would then coordinate the titanium site leading to an increase in the number of surface hydroxyl groups. As the newly formed hydroxyl groups are less stable than the initial doubly coordinated hydroxyl groups, the material restores its initial hydrophobicity in the space of a few hours after irradiation [52].

Different modes of electrospraying can be distinguished depending on the form of the meniscus, the pattern of motion of the jet, and the way it disintegrates into droplets [18]. In our particular case, the liquid was ejected directly from the capillary nozzle as a combination of regular large drops (dripping mode) and fine droplets (microdripping mode), although cone-jet modes were obtained when PEO was added to the solution. Fig. 4 shows SEM images of the electrosprayed coatings. The electrosprayed surface consisted of a well dispersed pattern of TiO_2 aggregates with grain size in the micron scale for the case of C(+) as shown in Fig. 4a. In the case of higher TiO_2 loadings, the surface details were mostly in the 100-200 nm range as shown in Fig. 4b and the detailed view of Fig. 4c. The reason for a different grain size and surface roughness is most probably the insulation due to the deposited layer of TiO_2, which would reduce the electrostatic force acting on the particles deposited on the outer layers of C(++) with respect to C(+) materials. The morphology of the drops was very similar in C(+) and C(++) samples. In some cases, the shape of the aggregates appeared distorted with axial elongation as a result of the stretching suffered by highly charged particles s shown in Fig. 4c with higher magnification [53,54]. The thickness of electrosprayed coatings is shown in Fig. 4d and e. Measurements taken on SEM micrographs yielded 3.2 μm and 4.3 μm respectively for C(+) and C(++) samples in good agreement with the TiO_2 surface density obtained for both types of

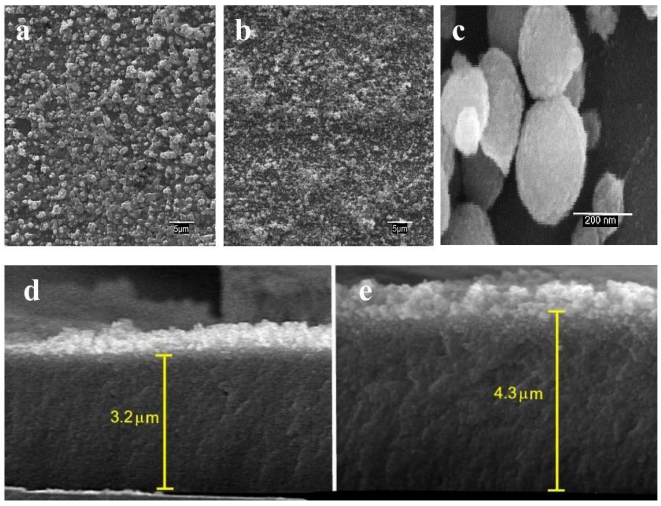

Figure 4. SEM images of TiO_2 electrospray coating of low TiO2 loading, C(+) (a), and high TiO_2 loading, C(++) (b and c) on glass coverslips. Cross-sectional micrographs of C(+) and C(++) samples (d and e respectively).

specimens. The fact that doubling the electrospray time does not increase layer thickness and surface density in the same proportion could also be attributed to the insulation effect of TiO_2 as it accumulates on glass covers.

3.3. Photocatalytic antibacterial effect

Two different sets of flow-cell photocatalytic assays were carried out with a total length of 24 h. In one set, the samples were incubated in the dark for 9 h, while the other was kept under the same conditions for 18 h. Samples, corresponding to the microbial colonization and biofilm growth were taken after the dark growth period for some measurements while other specimens were subsequently irradiated with the Xe-arc lamp mentioned before for 15 or 6 h, depending on the case, to complete the 24 h (9 + 15 or 18 + 6) contact with the bacterial culture in flow regime. These conditions were created to simulate the light-dark cycles that can be typically encountered in summer and winter conditions in average latitudes. In both assays cell viability and biofilm quantification was assessed by Live/Dead bacterial viability. Fig. 5 shows confocal images for Live/Dead bacterial viability staining on control coverslips without photocatalyst coating, C(-), and coverslips electrosprayed with low, C(+), and high, C(++), TiO_2 surface coverage either for non-irradiated, L(-), and irradiated, L(+), samples. During the 9 h or 18 h dark period, the growth of *S. aureus* took place without significant cell impairment both in C(-) and in C(+) or C(++) TiO_2 coated samples. This is clearly revealed by the absence of red-marked (cell membrane-damaged) bacteria in Fig. 5a, b, c, g, h and i. Certain cells appeared yellowish in C(+)-L(-) and C(++)-L(-) samples (samples with TiO_2 but kept in the dark). Yellow cells are considered viable and the effect could be associated to the irradiation suffered during confocal microscopy observations [55]. Conversely, the presence of the photocatalytic material drastically reduced the viability of the cells on TiO_2 coated coverslips under Xe-arc irradiation, as noted by the reduction of the number of cells and by the fact that the few remaining were clearly PI-marked as non-viable ones (Fig. 5e, f, k and l). The highest cell impairment was observed in C(++) samples after 15 h of irradiation, while Xe-arc lamp irradiation did not induce significant bacterial damage in the absence of TiO_2(Fig. 5d and g). Previous researches revealed that the cause for visible light damage in bacterial cells exposed to photocatalytic irradiated material was the production of reactive oxygen species (ROS) as intermediates of oxygen-dependent photosensitized reactions [12,56-59]. The photocatalytic action and the oxidative damage trigger the decreased expression of a large array of genes and proteins specific for regulatory, signaling and growth functions, in parallel with effects on coenzyme-independent respiration, cell wall structure and ion homeostasis [30,60]. However, the most evident damage induced by oxidative radicals is the disruption of cell defense barriers [59]. The damage induced by ROS on cell wall and membranes efficiently impairs bacterial at relatively low exposures. After the irradiation periods used in this study (6 h and 15 h), *S. aureus* cells were completely membrane damaged as shown by the complete absence of green-stained cells in the C(+) L(+) and C(++) L(+) samples (Fig. 5).

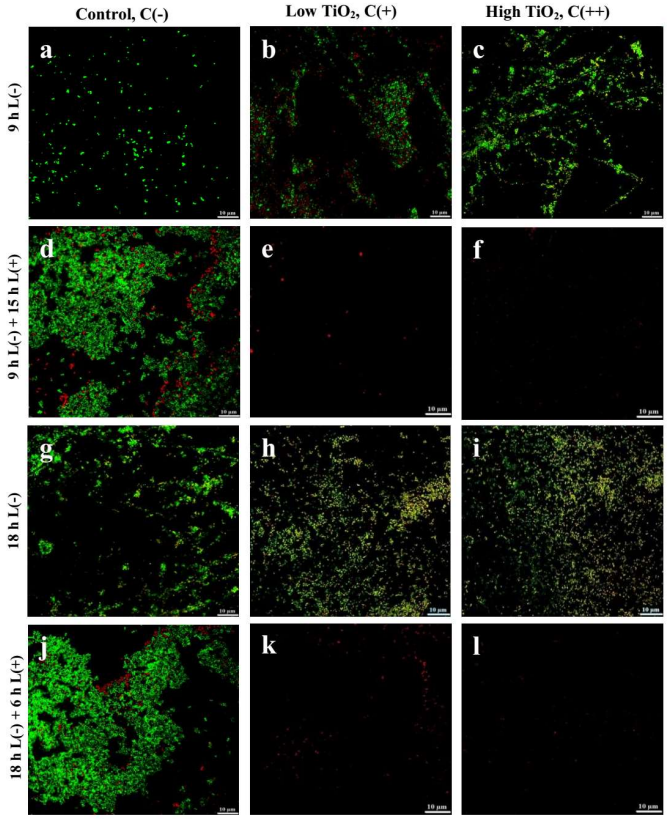

Figure 5. Live/Dead confocal micrographs of *S. aureus* on non-coated control C(-) (a, d, g and j) and TiO2 electrosprayed coverslips with low, C(+) (b, e, h and k) and high, C(++) (c, f, i and l) surface coverage. Irradiated and non-irradiated samples are denoted by L(+) and L(-) respectively. Dark period: 9 h and 18 h. Irradiation time: 15 h and 6 h. Scale bar: 10 μm.

The total amount of biomass on the surface of TiO_2 coated and uncoated coverslips was quantified by crystal violet staining before and after the dark incubation and after Xe-arc irradiation as described before. The results are shown in Fig. 6, in which the bars correspond to relative biofilm formation (the unity for uncoated and non-irradiated control) together with their 95% confidence intervals. In both flow-cell biofilm assays, the amount of biofilm formed after dark incubation (9 h or 18 h), was higher for samples with high TiO_2loading, particularly for the longer incubation time (18 h). However, after irradiation the amount of biomass accumulated on the surface of the photocatalyst coated samples decreased ~80% for C(+), and ~90% for C(++) with a minor influence of the

irradiation time. Noteworthy, TiO_2 covered samples kept 9 or 18 h in the dark experienced a higher biofilm growth, most probably as a consequence of the higher roughness of TiO_2 electrosprayed surfaces. Biofilm formation increased in all cases on uncoated controls due to the lack of the harmful effect of irradiation in the absence of photocatalytic material on their surface. It is interesting to note that the biofilm formation on C(++) samples was statistically non-significantly as the confidence intervals of the relative biofilm formation included zero.

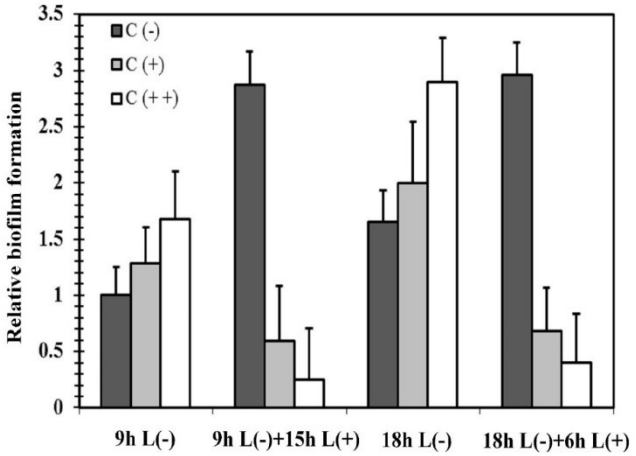

Figure 6. Quantification of biofilms by crystal violet in control coverslips C(-) (dark grey bars); low C(+) (light grey bars) and high C(++) (white bars) TiO_2 loadings, for non-irradiated L(-) and irradiated L(+) samples. Dark period: 9 h and 18 h. Irradiation time: 15 h and 6 h.

The quantification of bacteria removal in biofilms poses important difficulties. One reason is that bacteria in biofilms have an inherent lack of susceptibility to stressors compared to planktonic cultures of the same bacteria, which leads to significant errors when using conventional colony counting upon plating cultures. Also because of the need to resuspend bacterial cells measuring colony forming units [61]. The staining technique based on crystal violet provides a good measure of biofilm mass but does not give a measure of biofilm viability as it stains both live and dead bacterial cells. Live/dead staining is a useful method with the disadvantage that that only a small section of the biofilm can be assessed at a time [62]. In this work, the result can be interpreted in the light of Live/Dead staining, which showed that the few resulting cells after irradiation were clearly marked in red and, therefore, can be considered dead (Fig. 5). Consequently, the optical density measured with the crystal violet staining allowed estimating bacterial removal rates, which were: 54% and 66% for C(+) in 9h L(-) + 15h L(+) and 18h L(-) + 6h L(+) specimens respectively and 99% and 83% for C(++) in the cases of 9h L(-) + 15h L(+) and 18h L(-) + 6h L(+) runs. Additionally, after the irradiation periods, representative samples were again incubated in fresh nutrient medium (NB) under stirring for 24 h in darkness. Subsequently, the optical density of the culture was measured at 600 nm and plate count was performed to determine the recovery of any possible live cell. The results showed $DO_{600\ nm} < 0.05$ and a complete absence of colony forming cells.

Fig. 7 shows the information provided by FilmTracer SYPRO Ruby staining, a fluorescent marker that preferentially binds proteins, which are the components providing structural stability to biofilms. The biofilm formation was apparent in all non-irradiated samples, the higher amount of extracellular matrix (in red in Fig. 7) being that on TiO_2 electrosprayed surfaces during dark exposures. C(++) samples displayed higher matrix development and in the in the case of irradiated samples, biofilm formation was almost completely eliminated, particularly for C(++) samples irradiated for 15 h.

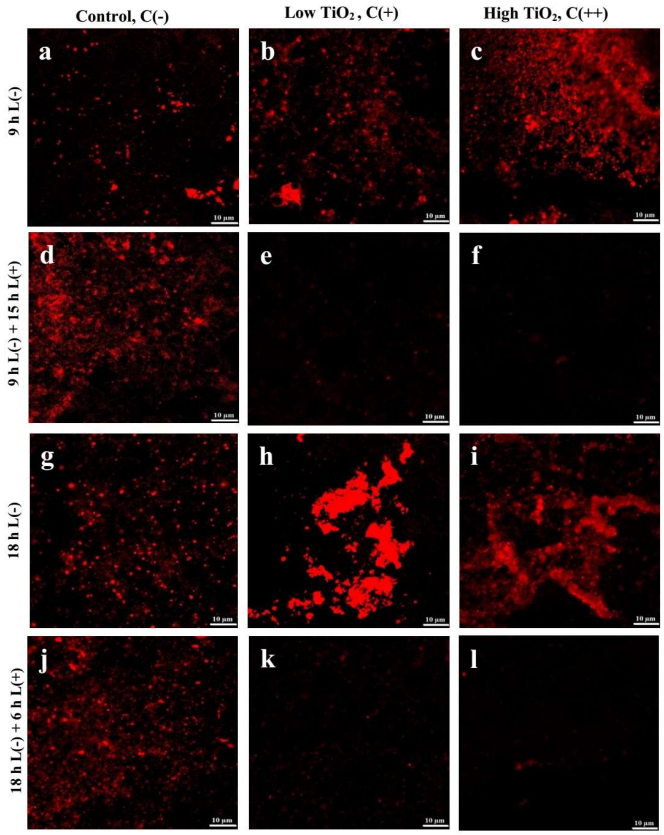

Figure 7. FilmTracer SYPRO Ruby biofilm matrix staining confocal micrographs of *S. aureus* on control coverslips C(-), (a, d, g and j); low C(+) (b, e, h and k) and high C(++) (c, f, I and l) surface coverage on TiO_2 electrosprayed coverslips. Irradiated and non-irradiated samples are denoted by L(+) and L(-) respectively. Dark period: 9 h and 18 h. Irradiation time: 15 h and 6 h. Scale bar: 10 µm.

It is widely accepted that highly polar surfaces repel due to the strongly bound hydration water, while less polar hydrophilic surfaces attract because hydrogen bonds between water molecules are favored with respect to surface hydration [63]. On the other hand, the attraction of hydrophobic surfaces, which actually attract water with considerable binding energy, is due to

the hydrogen-bonding free energy of cohesion of the water molecules of the liquid medium [64]. Accordingly, the maximum interaction expected between two surfaces takes place if the difference in hydrophilicity is not high because otherwise, adsorbed water molecules would lead to a net repulsion force. Bacterial adhesion consists of an initial attraction between cells and surface followed by the attachment and formation of adhesion structures. In our case, the surface ζ-potential of electrosprayed coatings was essentially neutral at neutral pH as shown in Table 1. Therefore, in the absence of electrostatic interactions with the negative surface charge of bacterial coatings, bacterial adhesion should be dominated by hydrophobic attractive forces [65]. The result is that hydrophobic bacteria tend to prefer hydrophobic substrates, while hydrophilic bacteria attach better to hydrophilic surfaces and generally hydrophobic bacteria adhere to a greater extent than hydrophilic bacteria [66].

In our work, we obtained higher amount of biofilm on surfaces covered by TiO_2 as long as they were kept in the dark. As described previously, TiO_2 coated surfaces displayed moderate hydrophilicity and were more easily colonized than bare coverslips during the dark exposure to bacterial cells, which also displayed a hydrophilic character, with a WCA of 21.8° ± 4.6° measured on bacterial lawns deposited on cellulose acetate filters. This is clearly observed in Fig. 6 and in revealed by the higher amount of extracellular matrix formed in C(++) samples in Figs. 7c and i. This fact is consistent with the slightly more hydrophilic character of TiO_2 with respect to bare glass coverslips, but it is more probably related to the higher roughness (Fig. 4) offered by TiO_2-electrosprayed surfaces compared to the smooth surface of the uncoated samples [67]. In support for this hypothesis it has been shown that the adhesive behavior of bacterial cells depends on the existence of cell surface structures, which result in steric and bridging effects due to the presence of cell appendages, including pili and flagella (Fig. 8g, h and i) as well as the EPS matrix segregated during biofilm formation, this interaction being favored in the case of rough surfaces [68]. The rationalization of bacterial attachment to surfaces is difficult in terms of pure physicochemical interactions by at least another two reasons. First, the adhesion process is sensitive to the physiological properties of the bacterium, which are strongly dependent on environmental factors [63]. Second, cell binding is affected by the culture media used due to differences in surface tension or the absorption of organic and inorganic compounds, which modify the way microorganisms adhere [69]. Additionally, the physicochemical characteristics of photo-responsive surfaces can be modified by the irradiation potentially leading to drastic changes in the ability of microorganisms to colonize them [70].

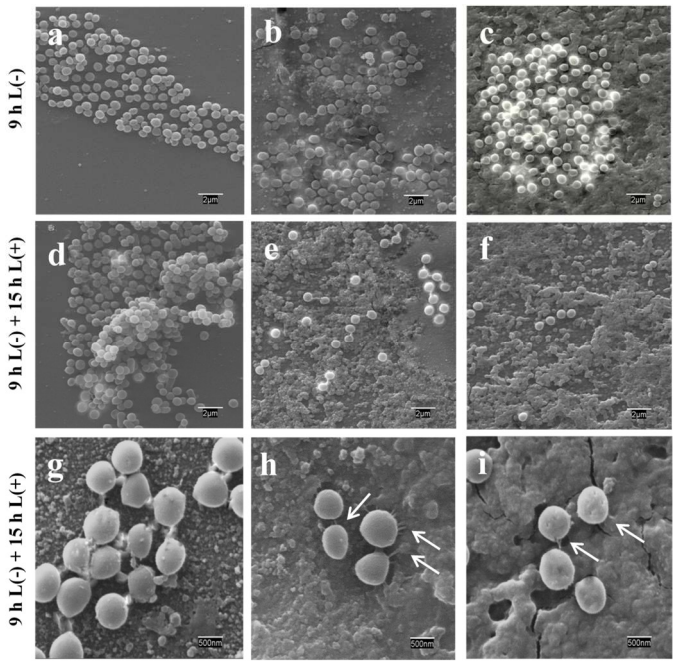

Figure 8. Representative SEM micrographs of *S. aureus* on control coverslips C(-) (a and d); low C(+) (b and e) and high C(++) (c and f) TiO_2 electrosprayed coverslips, for non-irradiated L(-) (a, b and c) and irradiated L(+) (d-i) samples. Images g, h and I show bacterial adhesion structures involved in biofilm formation in C(+) (g and h) and in C(++) samples (i). Dark period: 9 h. Irradiation time: 15 h.

The reduction of biofilm forming bacteria on TiO_2 photocatalytic surfaces has been widely described [68,71-73]. Apart from its effect on the integrity of cell envelopes, it is well-known that photocatalytic TiO_2 activity also has a negative effect in appendage biosynthesis and protein insertion as well as in cell signaling and cell to cell communication, which have been shown to play a role in diverse functions such as pathogenesis, biofilm development, stress resistance and cell survival [59]. In the case of biofilm removal, the most important parameters for cleaning efficiency are total biomass and living bacterial cells [74]. The presence of viable cells is critical as it enables fast recolonization if enough nutrients are available. In case of inefficient cleaning procedures, nutrients could come from dead bacterial cells and the remaining exopolysaccharides can be further used for bacterial adhesion and proliferation [75]. Our work showed that electrosprayed photocatalytic TiO_2 led to a complete removal of *S. aureus* cells with no viable microbial colonization according to Live/Dead staining results (Fig. 5) and no recovery of colony forming cells after the irradiation treatments in any case. For the TiO_2-covered electrosprayed surfaces, we showed that the irradiation following the contact with *S. aureus* cultures in the dark was enough to essentially eliminate the presence of biofilm structures, at least for the highest TiO_2 loading, C(++), while for C(+) some red-stained

polymeric matrix could be observed after irradiation (Fig. 7e and k). Considering both C(+) and C(++) surface were densely covered by TiO_2 as shown in Fig. 4, the difference explaining the higher activity of C(++) could be the lower size of particle aggregates in the top layer, that could lead to a higher efficiency in the photocatalytic formation of oxidative species. The results of crystal violet staining showed that the relative biofilm formation was not significantly different from zero in C(++) specimens, revealing that the ES TiO_2 deposition could effectively avoid the accumulation of biofilms in a flow-cell arrangement under conditions very favorable to bacterial growth like those used in this work. The surface loadings used in this work were inside the usual values reported for aqueous and gas phase TiO_2 photocatalytic surfaces, which are in the order of the mg cm^{-2} [76,77]. Consistent with these observations, The SEM images of C(++) assays after irradiation show only some dispersed cells with very few remaining adhesion structures (Fig. 8i), while for C(+) there were more cells attached to the surface and these structures were more clear (Fig. 8g and h) even after 15 h of irradiation. In sum, ES allowed producing homogeneous photocatalytic surfaces with the photochemical activity required to cope with the bacterial growth that could take place during dark periods under environmental exposures. The differences between C(+) and C(++) specimens revealed that surface physicochemical properties must be carefully considered to ensure an antibiofilm activity strong enough to avoid biofilm accumulation.

4. Conclusions

Suspensions of crystalline anatase nanoparticles prepared using a sol-gel synthesis were used to fabricate electrosprayed coatings on glass surfaces. The suspensions were stable, with ζ-potential in the 22.3-26.2 mV range and most particles exhibiting hydrodynamic diameters in the 13.5-15.8 nm range. The loading density and the thickness of the TiO_2electrosprayed layer were adjusted by using different electrospray times. The surface consisted of a pattern of aggregates ranging from the micron scale to the 100-200 nm range, with lower grain size for higher electrospray times, which could be attributed to the insulation produced by thicker layers of TiO_2.

Solar simulated irradiation was carried out using two different dark-light cycles in order to simulate different environmental conditions with an initial dark period to allow bacterial attachment from flowing cultures of *S. aureus*. The irradiation rendered all attached bacteria membrane damaged with no regrowth of cells in any case. The biomass removal was clear, reaching 99%. The irradiated surfaces were essentially free of bacterial exopolysaccharide matrix, particularly for specimens prepared with higher TiO_2 loadings. This work showed that ES technique can be efficient for creating active self-cleaning surfaces with precisely dispersed photocatalytic particles that can avoid biofilm accumulation even under stringent environmental conditions.

Acknowledgements

Financial support for this work was provided by the Spanish Plan Nacional de I+D+i through the project CTM2015-64895-R and CTM2013-45775 and the Dirección General de Universidades e Investigación de la Comunidad de Madrid, Research Network S2013/MAE-2716.

References

[1] T. Nonami, H. Hase, K. FunakoshiApatite-coated titanium dioxide photocatalyst for air purification. Catalysis Today, 96 (2004), pp. 113-118

[2] S. Malato, P. Fernández-Ibáñez, M.I. Maldonado, J. Blanco, W. Gernjak. Decontamination and disinfection of water by solar photocatalysis: recent overview and trends. Catalysis Today, 147 (2009), pp. 1-59

[3] G.J. Wang, S.W. Chou. Electrophoretic deposition of uniformly distributed TiO_2 nanoparticles using an anodic aluminum oxide template for efficient photolysis. Nanotechnology, 21 (2010), p. 115206

[4] S. Banerjee, J. Gopal, P. Muraleedharan, A. Tyagi, B. Raj. Physics and chemistry of photocatalytic titanium dioxide: visualization of bactericidal activity using atomic force microscopy. Current Science, 90 (2006), pp. 1378-1383

[5] Y. Oka, W.C. Kim, T. Yoshida, T. Hirashima, H. Mouri, H. Urade, Y. Itoh, T. Kubo. Efficacy of titanium dioxide photocatalyst for inhibition of bacterial colonization on percutaneous implants. Journal of Biomedical Materials Research Part B: Applied Biomaterials, 86 (2008), pp. 530-540

[6] J. Chen, C.S. Poon. Photocatalytic construction and building materials: from fundamentals to applications. Building and Environment, 44 (2009), pp. 1899-1906

[7] D.B. Hamal, J.A. Haggstrom, G.L. Marchin, M.A. Ikenberry, K. Hohn, K.J. Klabunde. A multifunctional biocide/sporocide and photocatalyst based on titanium dioxide (TiO_2) codoped with silver, carbon, and sulfur. Langmuir, 26 (2009), pp. 2805-2810

[8] S. Swetha, S. Santhosh, R. Geetha-Balakrishna, Synthesis and comparative study of nano-TiO_2 over Degussa P-25 in disinfection of water. Photochemistry and Photobiology, 86 (2010), pp. 628-632

[9] A. Rincón, C. Pulgarin. Photocatalytical inactivation of *E. coli*: effect of (continuous–intermittent) light intensity and of (suspended–fixed) TiO_2 concentration. Applied Catalysis B: Environmental, 44 (2003), pp. 263-284

[10] B. Kim, D. Kim, D. Cho, S. Cho. Bactericidal effect of TiO_2 photocatalyst on selected food-borne pathogenic bacteria. Chemosphere, 52 (2003), pp. 277-281

[11] L. Rizzo. Inactivation and injury of total coliform bacteria after primary disinfection of drinking water by TiO_2 photocatalysis. Journal of Hazardous Materials, 165 (2009), pp. 48-51

[12] H.A. Foster, I.B. Ditta, S. Varghese, A. Steele. Photocatalytic disinfection using titanium dioxide: spectrum and mechanism of antimicrobial activity. Applied Microbiology and Biotechnology, 90 (2011), pp. 1847-1868
[13] A. Kubacka, M.S. Diez, D. Rojo, R. Bargiela, S. Ciordia, I. Zapico, J.P. Albar, C. Barbas, V.A.P. Martins dos Santos, M. Fernández-García, M. FerrerUnderstanding the antimicrobial mechanism of TiO_2-based nanocomposite films in a pathogenic bacterium. Scientific reports, 4 (2014), p. 4134
[14] H. Yoon, B. Joshi, S.H. Na, S.S. Yoon. Antibacterial activity and photocatalysis of electrosprayed titania films. Journal of The Electrochemical Society, 159 (2012), pp. H823-H827
[15] B. Li, B.E. Logan. The impact of ultraviolet light on bacterial adhesion to glass and metal oxide-coated surface. Colloids and Surfaces B: Biointerfaces, 41 (2005), pp. 153-161
[16] J. Gage, T. Roberts, J. Duffy. Susceptibility of Pseudomonas aeruginosa biofilm to UV-A illumination over photocatalytic and non-photocatalytic surfaces. Biofilms, 2 (2005), pp. 155-163
[17] S. Ciston, R.M. Lueptow, K.A. Gray. Controlling biofilm growth using reactive ceramic ultrafiltration membranes. Journal of Membrane Science, 342 (2009), pp. 263-268
[18] A. Jaworek, A. Sobczyk. Electrospraying route to nanotechnology: an overview. Journal of electrostatics, 66 (2008), pp. 197-219
[19] C.J. Hogan, K.M. Yun, D.-R. Chen, I.W. Lenggoro, P. Biswas, K. Okuyama. Controlled size polymer particle production via electrohydrodynamic atomization. Colloids and Surfaces A: Physicochemical and Engineering Aspects, 311 (2007), pp. 67-76
[20] S.U. Halimi, N.F.A. Bakar, S.N. Ismail, S.A. Hashib, M.N. Naim, H. Setyawan, W. Widiyastuti, S. Machmudah. Electrospray deposition of titanium dioxide (TiO_2) nanoparticles, AIP Conference Proceedings, AIP, 2014, pp. 57-62.
[21] S. Zhang, K. Kawakami. One-step preparation of chitosan solid nanoparticles by electrospray deposition. International Journal of Pharmaceutics, 397 (2010), pp. 211-217
[22] Y. Terada, Y. Suzuki, S. Tohno. Synthesis and characterization of TiO_2 powders by electrospray pyrolysis method Materials Research Bulletin, 47 (2012), pp. 889-895
[23] T. Matsubara, Y. Suzuki, S. Tohno. Synthesis and characterization of TiO_2 powders by the double-nozzle electrospray pyrolysis method. Part 1. Refinement and monodispersion of sprayed droplets Comptes Rendus Chimie, 16 (2013), pp. 244-251
[24] F. Huijing, R.A. Hoerr. Electrospray: Scaling-Up, in: S.E. Lyshevski (Ed.) Dekker Encyclopedia of Nanoscience and Nanotechnology, CRC Press, 2014, pp. 1-11.
[25] J.E. Nam, J.H. Kim, H.J. Jo, J.K. Kang, D.K. Hwang. Effect of Thickness of Electrosprayed TiO_2 Photoelectrode for application in transparent yellow color dye-sensitized solar cells. Journal of Nanoscience and Nanotechnology, 16 (2016), pp. 10597-10601
[26] B. Hu, B. Liu, Dye-sensitized solar cells fabricated by the TiO_2 nanostructural materials synthesized by electrospray and hydrothermal post-treatment. Applied Surface Science 358A (2105) 412-417.
[27] J. Su, G. Yang, C. Cheng, C. Huang, H. Xu, Q. Ke. Hierarchically structured TiO_2/PAN nanofibrous membranes for high-efficiency air filtration and toluene degradation. Journal of Colloid and Interface Science, 507 (2017) (2017), pp. 386-396
[28] A.K. Krella, A. Krupa, M. Gazda, A.T. Sobczyk, A. Jaworek. Protective properties of Al_2O_3 + TiO_2 coating produced by the electrostatic spray deposition method. Ceramics International, 43 (2017), pp. 12126-12137
[29] J. Tang, A. Gomez. Controlled mesoporous film formation from the deposition of electrosprayed nanoparticles. Aerosol Science and Technology, 51 (2017), pp. 755-765
[30] N. Ledala, B. Zhang, J. Seravalli, R. Powers, G.A. Somerville. Influence of iron and aeration on *Staphylococcus aureus* growth, metabolism, and transcription. Journal of Bacteriology, 196 (2014), pp. 2178-2189
[31] T.R. Garrett, M. Bhakoo, Z. Zhang. Bacterial adhesion and biofilms on surfaces. Progress in Natural Science, 18 (2008), pp. 1049-1056
[32] C. de la Fuente-Núñez, F. Reffuveille, L. Fernández, R.E. Hancock. Bacterial biofilm development as a multicellular adaptation: antibiotic resistance and new therapeutic strategies. Current opinion in microbiology, 16 (2013), pp. 580-589
[33] B. Jalvo, M. Faraldos, A. Bahamonde, R. Rosal. Antimicrobial and antibiofilm efficacy of self-cleaning surfaces functionalized by TiO_2 photocatalytic nanoparticles against *Staphylococcus aureus* and *Pseudomonas putida.* Journal of Hazardous Materials, 340 (2017), pp. 160-170
[34] S.Y. Ryu, J.W. Chung, S.K. Kwak. Dependence of photocatalytic and antimicrobial activity of electrospun polymeric nanofiber composites on the positioning of Ag–TiO_2 nanoparticles. Composites Science and Technology, 117 (2015), pp. 9-17
[35] D.H. Kim, M.A. Anderson, W.A. ZeltnerEffects of firing temperature on photocatalytic and photoelectrocatalytic properties of TiO_2. Journal of Environmental Engineering, 121 (1995), pp. 590-594
[36] A. Daerr, A. Mogne. Pendant_Drop: An ImageJ Plugin to Measure the Surface Tension from an Image of a Pendant Drop. Journal of Open Research Software, 4 (2016)
[37] A.G. Marín, I.G. Loscertales, A. Barrero. Surface tension effects on submerged electrosprays. Biomicrofluidics, 6 (2012), p. 044104
[38] G. Taylor. Disintegration of water drops in an electric field, Proceedings of the Royal Society of London A: Mathematical, Physical and Engineering Sciences, The Royal Society, 1964, pp. 383-397.
[39] J.F. De La Mora, I.G. Loscertales. The current emitted by highly conducting Taylor cones. Journal of Fluid Mechanics, 260 (1994), pp. 155-184
[40] V. Gundabala, N. Vilanova, A. Fernández-Nieves. Current-voltage characteristic of electrospray processes in microfluidics. Physical Review Letters, 105 (2010), p. 154503

[41] N.P. Vitko, A.R. Richardson, Laboratory Maintenance of Methicillin-Resistant *Staphylococcus aureus* (MRSA). Current Protocols in Microbiology 28 C:9C.2 (2013) C:9C.2:9C.2.1–9C.2.14.
[42] G. Wolfaardt, J. Lawrence, R. Robarts, S. Caldwell, D. Caldwell. Multicellular organization in a degradative biofilm community. Applied and Environmental Microbiology, 60 (1994), pp. 434-446
[43] B.B. Christensen, C. Sternberg, J.B. Andersen, R.J. Palmer, A.T. Nielsen, M. Givskov, S. Molin. Molecular tools for study of biofilm physiology. Methods in Enzymology, 310 (1999), pp. 20-42
[44] J.M. Allen, S.K. Allen, S.W. Baertschi. 2-Nitrobenzaldehyde: a convenient UV-A and UV-B chemical actinometer for drug photostability testing. Journal of Pharmaceutical and Biomedical Analysis, 24 (2000), pp. 167-178
[45] M. Fletcher. The effects of proteins on bacterial attachment to polystyrene. Journal of General Microbiology, 94 (1976), p. 404
[46] G.A. O'Toole. Microtiter dish biofilm formation assay, JoVE (Journal of Visualized Experiments) (2011) e2437-e2437.
[47] J.A. Tapia-Hernández, P.I. Torres-Chávez, B. Ramírez-Wong, A. Rascón-Chu, M. Plascencia-Jatomea, C.G. Barreras-Urbina, N.A. Rangel-Vázquez, F. Rodríguez-Félix. Micro-and nanoparticles by electrospray: advances and applications in foods. Journal of Agricultural and Food Chemistry, 63 (2015), pp. 4699-4707
[48] R. Wang, K. Hashimoto, A. Fujishima, M. Chikuni, E. Kojima, A. Kitamura, M. Shimohigoshi, T. Watanabe. Light-induced amphiphilic surfaces. Nature, 388 (1997), pp. 431-432
[49] N. Stevens, C. Priest, R. Sedev, J. Ralston. Wettability of photoresponsive titanium dioxide surfaces. Langmuir, 19 (2003), pp. 3272-3275
[50] R.D. Sun, A. Nakajima, A. Fujishima, T. Watanabe, K. Hashimoto. Photoinduced surface wettability conversion of ZnO and TiO_2 thin films. The Journal of Physical Chemistry B, 105 (2001), pp. 1984-1990
[51] M. Miyauchi, N. Kieda, S. Hishita, T. Mitsuhashi, A. Nakajima, T. Watanabe, K. Hashimoto. Reversible wettability control of TiO_2 surface by light irradiation. Surface Science, 511 (2002), pp. 401-407
[52] K. Hashimoto, H. Irie, A. Fujishima .TiO_2 photocatalysis: a historical overview and future prospects. Japanese Journal of Applied Physics, 44 (2005), p. 8269
[53] E. Scholten, H. Dhamankar, L. Bromberg, G.C. Rutledge, T.A. Hatton. Electrospray as a tool for drug micro-and nanoparticle patterning. Langmuir, 27 (2011), pp. 6683-6688
[54] K. Songsurang, N. Praphairaksit, K. Siraleartmukul, N. Muangsin. Electrospray fabrication of doxorubicin-chitosan-tripolyphosphate nanoparticles for delivery of doxorubicin. Archives of Pharmaceutical Research, 34 (2011), pp. 583-592
[55] L. Boulos, M. Prevost, B. Barbeau, J. Coallier, R. Desjardins. LIVE/DEAD® BacLight™: application of a new rapid staining method for direct enumeration of viable and total bacteria in drinking water. Journal of Microbiological Methods, 37 (1999), pp. 77-86
[56] P. Dunlop, C. Sheeran, J. Byrne, M. McMahon, M. Boyle, K. McGuigan. Inactivation of clinically relevant pathogens by photocatalytic coatings. Journal of Photochemistry and Photobiology A: Chemistry, 216 (2010), pp. 303-310
[57] A. Kubacka, M. Ferrer, M. Fernández-García. Kinetics of photocatalytic disinfection in TiO2-containing polymer thin films: UV and visible light performances. Applied Catalysis B: Environmental, 121 (2012), pp. 230-238
[58] J. Kiwi, V. Nadtochenko. Evidence for the mechanism of photocatalytic degradation of the bacterial wall membrane at the TiO_2 interface by ATR-FTIR and laser kinetic spectroscopy. Langmuir, 21 (2005), pp. 4631-4641
[59] A. Kubacka, M.S. Diez, D. Rojo, R. Bargiela, S. Ciordia, I. Zapico, J.P. Albar, C. Barbas, V.A.M. dos Santos, M. Fernández-García. Understanding the antimicrobial mechanism of TiO_2-based nanocomposite films in a pathogenic bacterium. Scientific Reports, 4 (2014), p. 4134
[60] G. Pishchany, K.P. Haley, E.P. Skaar. *Staphylococcus aureus* growth using human hemoglobin as an iron source. JoVE (Journal of Visualized Experiments) (2013) e50072-e50072.
[61] K. Welch, Y. Cai, M. Strømme. A method for quantitative determination of biofilm viability. Journal of Functional Biomaterials, 3 (2012), pp. 418-431
[62] M. Berney, F. Hammes, F. Bosshard, H.U. Weilenmann, T. Egli. Assessment and interpretation of bacterial viability by using the Live/Dead baclight kit in combination with flow cytometry. Applied Environmental Microbiology, 73 (2007), pp. 3283-3290
[63] M. Kanduc, E. Schneck, R.R. Netz. Attraction between hydrated hydrophilic surfaces. Chemical Physics Letters, 610–611 (2014), pp. 375-380
[64] C. Van Oss. Hydrophobicity of biosurfaces—origin, quantitative determination and interaction energies. Colloids and Surfaces B: Biointerfaces, 5 (1995), pp. 91-110
[65] Y.L. Ong, A. Razatos, G. Georgiou, M.M. Sharma. Adhesion forces between *E. coli* bacteria and biomaterial surfaces. Langmuir, 15 (1999), pp. 2719-2725
[66] O. Habimana, A.J.C. Semião, E. Casey. The role of cell-surface interactions in bacterial initial adhesion and consequent biofilm formation on nanofiltration/reverse osmosis membranes. Journal of Membrane Science, 454 (2014), pp. 82-96
[67] M. Katsikogianni, Y. Missirlis. Concise review of mechanisms of bacterial adhesion to biomaterials and of techniques used in estimating bacteria-material interactions. European Cells & Materials Journal, 8 (2004)
[68] K. Hori, S. Matsumoto. Bacterial adhesion: from mechanism to control. Biochemical Engineering Journal, 48 (2010), pp. 424-434
[69] C.J. van Oss. Hydrophobicity and hydrophilicity of biosurfaces. Current Opinion in Colloid & Interface Science, 2 (1997), pp. 503-512
[70] B. Jalvo, J. Santiago-Morales, P. Romero, R.G. de Villoria, R. Rosal. Microbial colonisation of transparent glass-like carbon films triggered by a reversible

radiation-induced hydrophobic to hydrophilic transition. RSC Advances, 6 (2016), pp. 50278-50287
[71] E.J. Wolfrum, J. Huang, D.M. Blake, P.-C. Maness, Z. Huang, J. Fiest, W.A. Jacoby. Photocatalytic oxidation of bacteria, bacterial and fungal spores, and model biofilm components to carbon dioxide on titanium dioxide-coated surfaces. Environmental Science & Technology, 36 (2002), pp. 3412-3419
[72] Y. Cai, M. Strømme, Å. Melhus, H. Engqvist, K. Welch. Photocatalytic inactivation of biofilms on bioactive dental adhesives. Journal of Biomedical Materials Research Part B: Applied Biomaterials, 102 (2014), pp. 62-67
[73] C.N. Rao, T. Takashima, W.A. Bradley, T.Y. Lee. Near ultraviolet radiation at the earth's surface: measurements and model comparisons. Tellus B, 36 (1984), pp. 286-293
[74] P. Stiefel, U. Rosenberg, J. Schneider, S. Mauerhofer, K. Maniura-Weber, Q. Ren. Is biofilm removal properly assessed? Comparison of different quantification methods in a 96-well plate system. Applied Microbiology and Biotechnology, 100 (2016), pp. 4135-4145
[75] S.E. Finkel, R. Kolter. DNA as a nutrient: novel role for bacterial competence gene homologs. Journal of Bacteriology, 183 (2001), pp. 6288-6293
[76] I. Salem, N. Keller, V. Keller. Photocatalytic removal of monoterpenes in the gas phase. Activity and regeneration, Green Chemistry, 11 (2009), pp. 966-973
[77] M. Kete, E. Pavlica, F. Fresno, G. Bratina, U.L. Štangar. Highly active photocatalytic coatings prepared by a low-temperature method. Environmental Science and Pollution Research, 21 (2014), pp. 11238-11249

SUPPLEMENTARY MATERIAL

Antibacterial surfaces prepared by electrospray coating of photocatalytic nanoparticles

Blanca Jalvo[1], Marisol Faraldos[2,*], Ana Bahamonde[2], RobertoRosal[1,*]

[1] Department of Chemical Engineering, University of Alcalá, E-28871 Alcalá de Henares, Madrid, Spain
[2] Instituto de Catálisis y Petroleoquímica, ICP-CSIC, Marie Curie 2, E-28049 Madrid, Spain

* Corresponding authors: mfaraldos@icp.csic.es, roberto.rosal@uah.es

Contents

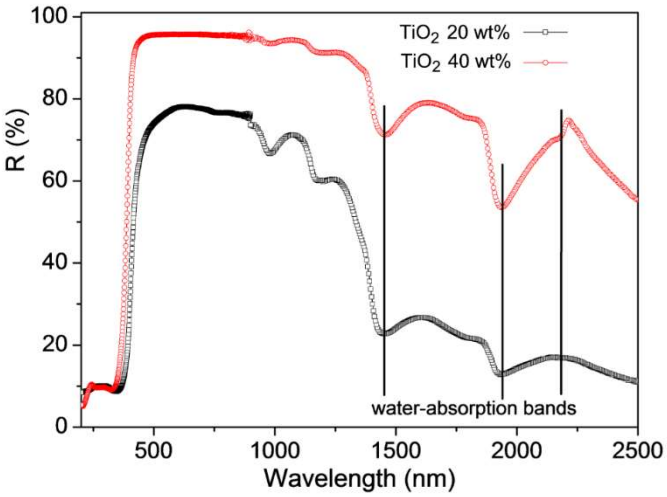

Figure. S1. UV-Vis-NIR spectra of TiO_2 A (20 wt%) and B (40 wt%) xerogels.

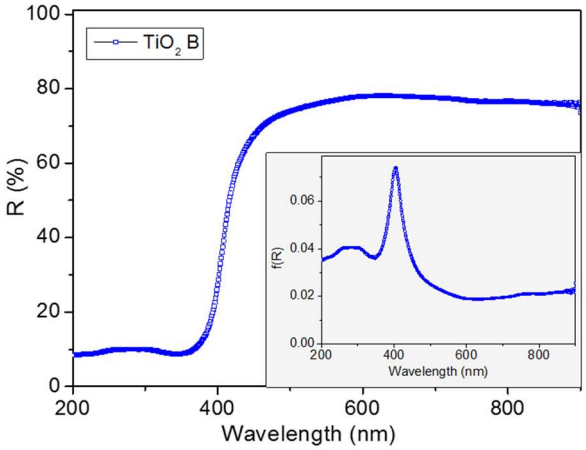

Figure. S2. UV-Vis Diffuse Reflectance spectrum of TiO_2 B deposited on coverslips.

TiO_2 A

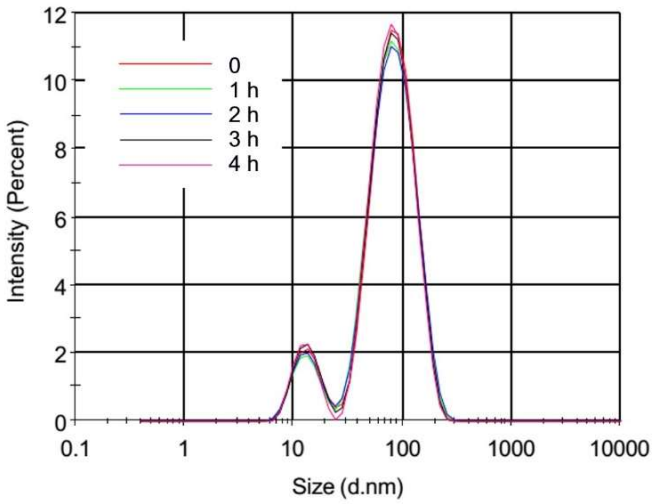

TiO_2 B

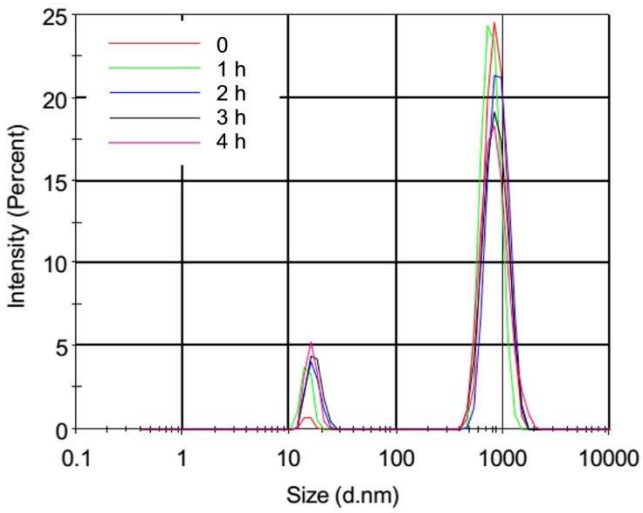

Figure. S3 DLS particle size measurements of TiO_2 A (20 wt%) and TiO_2 B (40 wt%) suspensions during a 4 h period.